Sensors & Actuators: B. Chemical 272 (2018) 502–509

Contents lists available at ScienceDirect

Sensors and Actuators B: Chemical

journal homepage: www.elsevier.com/locate/snb

A high sensitivity bead-based immunoassay with nanofluidic preconcentration for biomarker detection

Yu-Jui Fan[a,b], Chih-Zong Deng[c], Pei-Shan Chung[d], Wei-Cheng Tian[e,f,g], Horn-Jiunn Sheen[c,*]

[a] School of Biomedical Engineering, Taipei Meidical University, 250 Wuxing St., Taipei 11031, Taiwan, ROC
[b] International Ph.D. Program for Biomedical Engineering, Taipei Medical University, 250 Wuxing St., Taipei 11031, Taiwan, ROC
[c] Institute of Applied Mechanics, National Taiwan University, No. 1, Sec. 4, Roosevelt Road, Taipei 10617, Taiwan, ROC
[d] Department of Bioengineering, University of California Los Angeles, 420 Westwood Plaza, Los Angeles, CA 90095, USA
[e] Graduate Institute of Biomedical Electronics and Bioinformatics, National Taiwan University, No. 1, Sec. 4, Roosevelt Road, Taipei 10617, Taiwan, ROC
[f] Department of Electrical Engineering, National Taiwan University, No. 1, Sec. 4, Roosevelt Road, Taipei 10617, Taiwan, ROC
[g] Graduate Institute of Electronics Engineering, National Taiwan University, No. 1, Sec. 4, Roosevelt Road, Taipei 10617, Taiwan, ROC

ARTICLE INFO

Keywords:
Nanofluidic preconcentrator
Brownian motion
Micro-PTV
Bead-immunoassay

ABSTRACT

In this study, we developed a rapid biomarker sensor with a high sensitivity and high selectivity by applying a bead-based immunosensing technique in a nanofluidic preconcentration device. Antibody-coated 300-nm beads and antigens were mixed and then pumped into a valve-integrated nanofluidic preconcentration device for collection and trapping. Because of size differences between the molecules and 300-nm beads, the antigen (molecule) in the mixed solution could be concentrated by up to 10,000-fold in 2 min, but the nanobeads could not be thus concentrated. After concentrated antigens and antibody-coated nanobeads were isolated, micro-particle tracking velocimetry was used to measure the Brownian diffusion of the nanobeads in real time to determine the antigen concentration. Through this preconcentration experiment, we demonstrated a rapid and high-sensitivity detection of prostate-specific antigen with a detection limit of 50 pg/ml in 20 min.

1. Introduction

Prostate-specific antigens (PSAs), first found in human prostate tissues and human serum in 1971, are the most favorable biomarkers currently available for detecting prostate and breast cancers [1]. The PSA concentration in a healthy person ranges from 0 to 4 ng/ml. The quantitative detection of PSA is typically performed using conventional immunoassays, including enzyme-linked immunosorbent assay (ELISA) [2], radioimmunoassay, and chemiluminescence assay; in addition, optical methods including fluorescent labeling [3,4] and surface-enhanced Raman scattering [5] are reliable and have sufficient sensitivity and selectivity. However, certain challenges remain to be addressed, such as miniaturization, reaction time reduction, fabrication step simplification, and cost reduction. To detect biomarkers at low concentrations, the ELISA requires a longer reaction time and multiple rinsing and mixing processes. Certainly, most such tests must be conducted in a dedicated place with large, automatic analyzers, which presents problems such as sample transportation and administration, increased waiting time, and increased medical costs. Simple, rapid, low-cost, reliable, and affordable PSA measurement methods with miniaturized systems are required.

To overcome these problems, many signal transducers have been developed using bulk components and high-cost optical detection methods for PSA immunoassays, such as surface plasmon resonance biosensors [6], microcantilever beams [7], electrochemical sensors [8], silicon nanowire field-effect transistors [9], gold nanowire immunosensors [10], and single-walled carbon nanotube-based biosensors [11,12]. However, most of these on-chip transducers require complicated fabrication procedures or involve highly specific conjugation processes to achieve pg/ml levels of sensitivity and selectivity for PSA detection. This implies that the devices may be costly, and multiple reaction steps require considerable time.

Recently, another approach to enhancing the sensitivity of immunoassays was proposed; it uses a nanofluidic preconcentrator, which detects low-abundance PSA and achieves pg/ml concentrations [13]. A nanoscale porous membrane [14] and parallel nanofluidic channels [15] have been used as ion-selective channels to deplete ions for blocking proteins, and a million-fold protein concentration has been demonstrated in 30 min [16]. By using a dual-loop circuit model, the generation time and location of the protein plug can be predicted with labels, and the protein plug can be manipulated by tuning the voltages of the two circuits [17]. Nanofluidic concentration devices have been

* Corresponding author.
E-mail addresses: sheenh@ntu.edu.tw, sheenh@spring.iam.ntu.edu.tw (H.-J. Sheen).

https://doi.org/10.1016/j.snb.2018.05.141
Received 15 August 2017; Received in revised form 1 May 2018; Accepted 24 May 2018
Available online 01 June 2018
0925-4005/

successfully developed to continuously collect charged molecules in a given sample and trap them into a much smaller volume, thus significantly increasing the local protein concentration. These devices have been used to enhance surface-bound protein binding kinetics [18] and increase the sensitivity of homogeneous enzymes [19,20]. Nanofluidic preconcentration devices integrated with a valve were developed to trap protein plugs for static immunoassays [21]. Although the immunoassay's sensitivity improved when a preconcentrator was used, the time taken for molecules to diffuse to the channel surface for antibody–antigen interactions remained high.

Our group developed a quantitative three-dimensional (3D) nanobead immunoassay in which diffusion variations in antibody-coated nanobeads in an analyte solution can be measured in real time through micro particle tracking velocimetry (micro-PTV) [22,23]. When the antibody-coated nanobeads are conjugated with an antigen, the diffusivity of the nanobeads decreases. Unlike conventional immunoassays in which antibody–antigen interactions occur at the boundary surface, the reactions in a nanobead immunoassay occur in free space, which allows Brownian movement to accelerate collisions of nanobeads and analytes. The nanobead immunoassay has been demonstrated for viral [24–26] and molecular [27,28] detection.

A possible approach to low-abundance analyte sensing is to preconcentrate a sample through electrokinetic trapping (EKT), which traps molecules in a microscopic volume through ion concentration polarization [29] and electroosmotic flow (EOF) control. This method can achieve a high level of sample preconcentration (approximately several million-fold) and is suitable for any molecule or cell with a charge opposite to the surface charge of the ion-selective channels [16]. Recently, a dual-loop design of a concentrator was proposed to trap molecules and to manipulate the preconcentrated plug in a microfluidic channel for various further uses [17].

In this study, we integrated a bead-based immunoassay with a dual-loop nanofluidic preconcentration device for rapid and high-sensitivity biomarker detection. The valve-integrated dual-loop nanofluidic preconcentration device is presented in Fig. 1(a), and a schematic of the design of the pneumatic valve is presented in Fig. 1(b). The dual-loop circuit design for label-free preconcentration prediction and manipulation is presented in Fig. 1(c). A pair of push-down type pressurized valves near a Nafion membrane can completely block the semi-pipe channel and trap the collected proteins between the valves. First, antibody-coated nanobeads mixed with sample solutions are injected into the channel as shown in Fig. 1(d), and then the device concentrates the nanobeads for several minutes as shown in Fig. 1(e). After a concentrated protein plug is formed, the pneumatic valves are pressurized to trap the collected proteins and antibody-coated nanobeads, as shown in Fig. 1(f), for further 3D bead immunosensing. The antibody–antigen interaction decreases the nanobeads' Brownian diffusivities as shown in Fig. 1(g), thus allowing the quantification of the enriched antigen concentration by comparison with reference results.

2. Experimental

2.1. Preparation of antibody-coated nanobeads

Carboxyl functional group ($COOH^-$)-modified 300-nm nanobeads (XC030, Merck), with respective optical excitation and emission wavelengths of 475 and 525 nm, were used in this experiment. The density of the beads was approximately 1.05 g/cm^3, and the surfaces of the beads carried a negative charge, which enabled them to remain suspended in the liquid without sedimentation.

The anti-PSA (SAB1303590, Sigma-Aldrich Co.) was conjugated with carboxyl functional groups by following a well-known protocol for efficient two-step coupling by using 1-ethyl-3-(3-dimethylaminopropyl) carbodiimide (EDC) (22980, Thermo Fisher Scientific Inc.) and N-hydroxysuccinimide (NHS) (130672, Sigma-Aldrich Co.). First, the EDC cross linker reacted with NHS to increase the coupling efficiency. When the nanobeads had been modified with EDC, the nanobeads and anti-PSA were linked using EDC-NHS.

2.2. Bead-based immunoassay by measuring nanobeads' Brownian diffusivities

Brownian diffusion, the random motion of particles suspended in a liquid, results from the collisions of atoms, molecules, and particles. Brownian motions of nanobeads mainly depend on particle sizes, environment temperature, and solution properties. During a bead-based immunoassay, the sizes of the nanobeads increase when the antigens conjugate onto their surfaces. This process decreases the Brownian diffusivities of the nanobeads. By measuring the Brownian diffusivities of the immunobeads before and after antigen conjugation, the concentration of the sample can be quantitatively determined [22].

2.3. Valve-integrated nanofluidic preconcentrator

In this experiment, our nanofluidic preconcentration device comprised two microfluidic channels connected by ion-selective nanoporous membranes composed of Nafion (70160, Sigma-Aldrich Co.). First, the Nafion was dissolved in a mixture of lower aliphatic alcohols and water; then it was patterned on a glass substrate by using a polydimethylsiloxane frame. The patterned thin Nafion membrane was successfully deposited on the substrate after solution volatilization. To create pneumatic valves on the device, the cross section of the microfluidic channels was designed in an arc shape to enable the deformable thin film on the flat side of the microfluidic channels to be pressurized and deformed for perfect attachment to the inner arc well of the channels. The other side of the thin film was bound to a chamber with a single inlet, which was connected to a pressure source, Fig. 1(a) and (b).

Initially, the cations (positive ions) and anions (negative ions) are uniformly distributed inside the microfluidic channel as in Fig. 1(h). When voltages are applied to this preconcentration device, the EOF-induced ion flow moves along the electric field as Fig. 1(i). The ion concentration polarization effect, which is an electrochemical transport phenomenon occurring near ion-selective channels upon the passage of an electric current, is induced near the junction between the operating channel and the nanoporous membrane. Because of the electrokinetic effects in microchannels or nanochannels [30,31] and the presence of negative or positive ions [16], a depleted diffusion layer and an enriched diffusion layer appear at the locations with the highest and lowest electric potential in the ion-selective channels, respectively. This phenomenon is also called the ion depletion/enrichment process[29]. In this experiment, we are interested in the depletion region because of ion blocking phenomenon as Fig. 1(j).

The ion depletion region can be used to trap the proteins and molecules that are carried by EOF; this effect is called EKT as Fig. 1(k). At the beginning of the experiment, the total amount of proteins can be drastically increased within a short period in a tiny space adjacent to the depletion region to form a protein plug. In the next step, the protein plug can be preserved between a pair of pneumatic valves. This replaces EKT, and thus, the applied voltage is not required.

2.4. Experimental setup

Fig. 2 presents the experimental setup of this system. In this dual-loop nanofluidic preconcentration system, two picoammeter/voltage sources (Model 6487, Keithley Instruments Inc.) were used to separately provide the electrical voltages for the left and the right circuits. To supply voltages to and monitor currents in these two loops, a NI-VISA interface (NI Labview, National Instruments Corp.) was used in addition to general purpose interface bus (GPIB) controllers, (GPIB-USB-HS, National Instruments Corp.) to control GPIB instruments. The protein concentration process was observed using an inverted epi-fluorescence microscope (IX71, Olympus Co.) with a 10X objective lens,

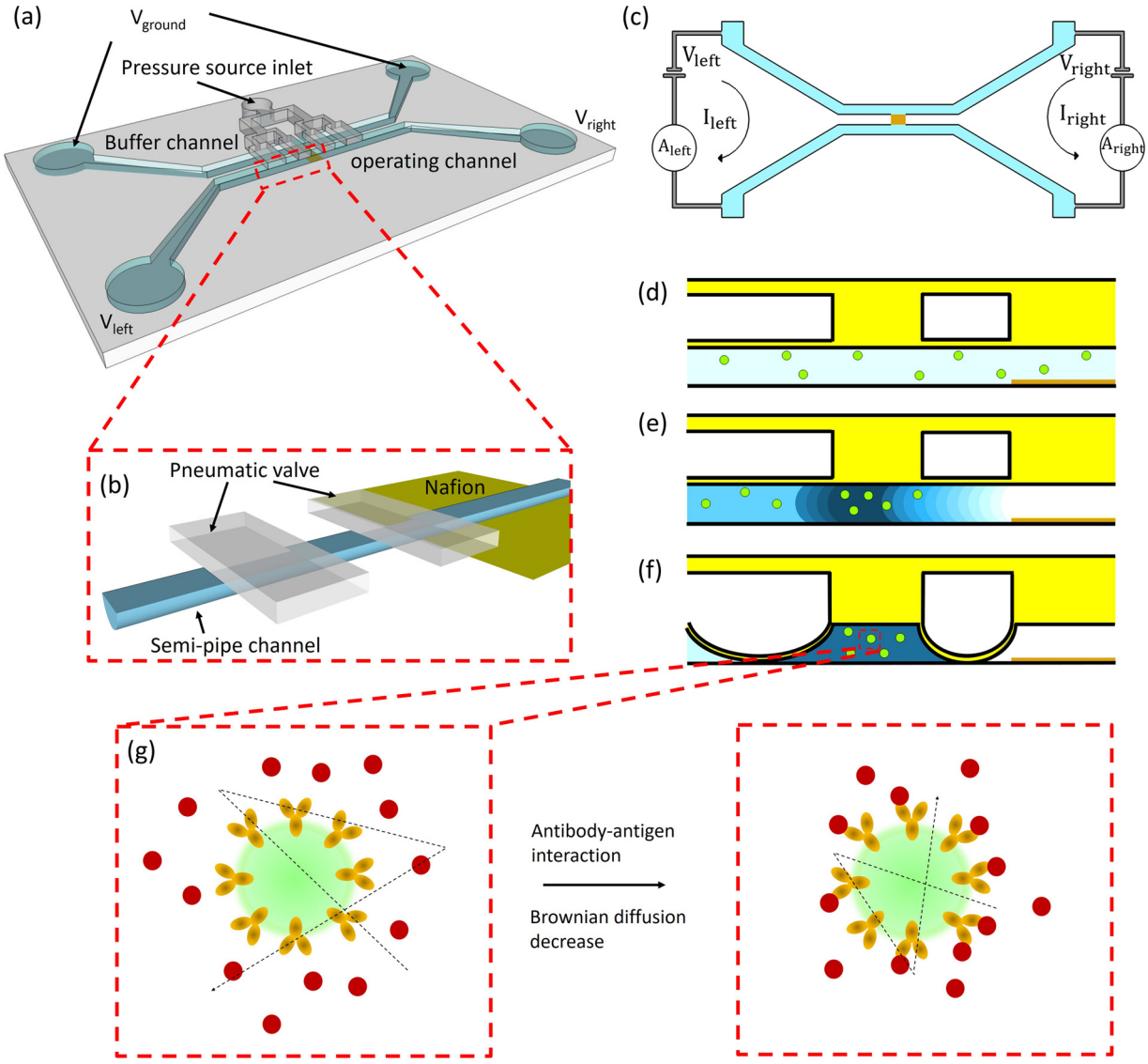

Fig. 1. (a) Schematic of the nanofluidic concentrator with pneumatic valves for isolating immunobeads and the concentrating plug. (b) The pneumatic valve and semi-pipe device can be fabricated by multilayer microfluidic fabrication process. (c) The dual-loop circuit design can be used to predict and manipulate the molecular concentration in the operation channel. Mixed samples can be (d) injected, (e) concentrated, and (f) trapped in the device. (g) The antigens interact with antibody-modified nanobeads and this phenomenon leads to that the nanobeads' Brownian diffusivities decrease.

and was captured using a charge-coupled device (CCD) camera (DXC-190, SONY). For bead immunoassay by measuring the Brownian diffusion in nanobeads, sequential images of isolated nanobeads were acquired using another CCD camera (PowerView plus 2 M, TSI Inc.). Micro-PTV software (Insight 3G™, TSI Inc.) was used to analyze the behavior and diffusivity of nanobeads. To control the pneumatic valves on our device, a pressure source was connected through a three-way switch.

3. Results and discussion

In the preconcentration-enhanced biosensing technique, antibody-coated nanobeads and antigen solutions with different concentrations were first mixed and pumped into the device. The preconcentrated plug in the device was manipulated by tuning the voltages of the left and right circuits, and a pair of pneumatic valves were pressurized to block the channel and isolate the concentrated antigens and antibody-coated nanobeads. The currents in the left and right circuits were measured. The concentration process can be described in step-by-step detail as follows.

3.1. Performance of nanofluidic preconcentrator and valves

To visualize the concentration process, 5.8 nM fluorescent-labeled goat anti-mouse IgG (31569, Thermo Fisher Scientific) was added to phosphate buffered saline at a pH of 7.8. The solution was injected into the microfluidic channel in advance by using a syringe pump (Fusion 200, Chemyx). The operation processes of protein concentration in the microfluidic channel and the protein concentration of the plug trapped by pneumatic valves are depicted as sequential images of different stages of the concentration and trapping periods in Fig. 3(b). According to our previous study [17], each stage of the nanofluidic concentration process can be described by monitoring dual-loop currents. These sequential images are also presented on a current–time curve in Fig. 3(c).

To determine the characteristic voltages in the concentration process of the dual-loop preconcentrator device, the supplied voltages were swept from 5 to 70 V until the concentration process was initiated and finally completed. Initially, when no voltage was supplied, the fluorescent protein could not be observed in the operating channel because the fluorescence intensity was too low [Fig. 3(b)-i]. To initiate the concentration process ($t = 0$), an initial voltage of 5 V and a step

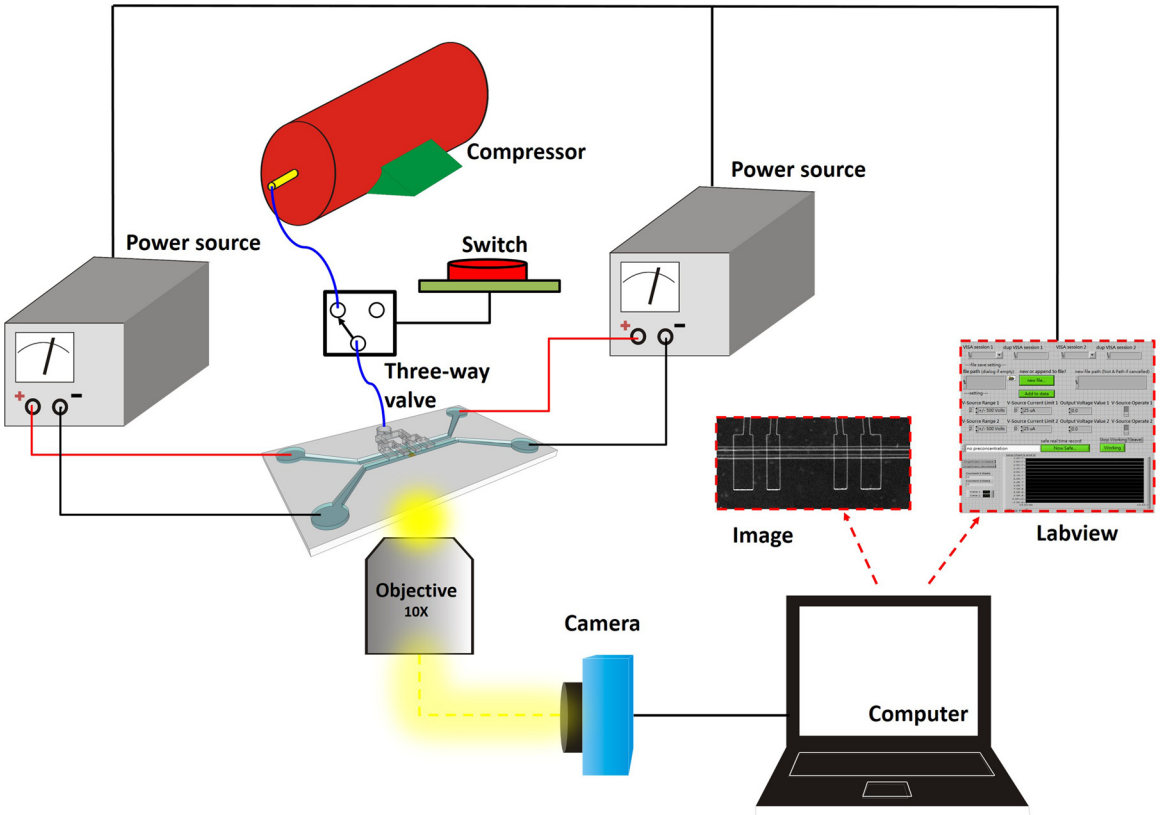

Fig. 2. Experimental setup. Two power sources controlled using LabVIEW were used to drive the preconcentration device. A compressor was used to generate high pressure air to pressurize pneumatic valves. An image system was used to monitor microfluidic behaviors in the microfluidic channel.

voltage of 1 V per 7 s were supplied to V_{left} and V_{right}. The currents in the left (I_{left}) and right (I_{right}) loops began to deviate until the supplied voltages reached 21 V (t = 110 s). This phase is called the separation period. In this experiment, I_{left} was larger than I_{right}, which indicated that the volume flow rate from the left-hand side of the microfluidic channel to the depletion region was greater than that from the right-hand side. The experimental results indicated that the concentration process on the left side of the depletion region was faster than that on the right side. At t = 110 s, the depletion region was fully developed and blocked the operating channel, Fig. 3(b)-ii. Both the right- and left-loop currents decreased because of the onset of the EKT mechanism, which led to nanoporous membrane-induced backflow.

As V_{left} and V_{right} were further increased, the fully developed depletion region began to trap protein molecules and form a concentration plug; this phase is called the plug-appearance period. At t = 110–380 s, the left-loop current continuously increased because of the higher number of ions being transported per unit time from the left-hand-side reservoir and the channel passing through the nanoporous membrane. Furthermore, the right-loop current continuously decreased because fewer ions were passing through the nanoporous membrane per unit time in the direction opposite to the upper-stream direction. Plug concentration occurred at the higher current side of the two loops. The proteins were collected on the left side of the depletion region, Fig. 3(b)-iii.

The protein plug can be moved to and trapped between a pair of pneumatic valves through manipulation processes, including voltage-controlled depletion region manipulation, pressurized plug squeezing, and plug isolation by using two fully closed pneumatic valves. To manipulate the protein plug trapped through the EKT mechanism, we adjusted the applied voltages of the two circuits. When the same voltages were applied to the left and the right circuits, the EKT mechanism was initiated once the tangential electric potential gradients in the depletion region contributed to the electroosmotic force and nanoporous backflow. Therefore, when a voltage difference occurred, the depletion region developed bias toward the higher voltage side. Because of this phenomenon, the concentration plug was also pushed toward the higher voltage side. In this experiment, the concentration plug was initially located on the left side of the depletion region. By application of higher voltage to the left circuit, the concentration plug was manipulated to move toward the left side. However, the moving distance was limited because the applied voltage was required to remain below a particular limit for the following three reasons. First, a high electric potential gradient leads to a high electroosmotic force, which renders the current densities regularly or irregularly unstable [32]. Second, breakdown voltage of the microfluidic/nanofluidic channel junction gap occurs when the given voltage is too high [33], thus destroying the structure and altering the characteristics of the chip [17]. Third, high voltage-induced electric potential gradients may influence the conformations and related properties of the biomolecules and generate excessive heat and gas bubbles near the operational electrodes [34].

By control of the driving voltage, the protein plug was pushed toward the reaction chamber from the valve 2 region, Fig. 3(b)-iv. Moreover, the protein plug was at most pushed to the region near the interface between the reaction chamber and valve 2 region since the driving voltage was limited, as previously mentioned. Furthermore, by pressurizing the pneumatic valves, the protein plug was squeezed into the reaction chamber, which is the space between valves 1 and 2. Simultaneously, the right and left circuits became open circuits because the ion flows were completely blocked, and the EKT force vanished. Consequently, the isolated proteins and molecules could homogeneously diffuse in the entire reaction chamber region, as depicted in Fig. 3(b)-v. The formation, movement, and trapping of the protein plug are also indicated in the real-time current diagram, Fig. 3(c). The characteristic driving voltages and their corresponding operating periods in our preconcentration experiments are described in the figure

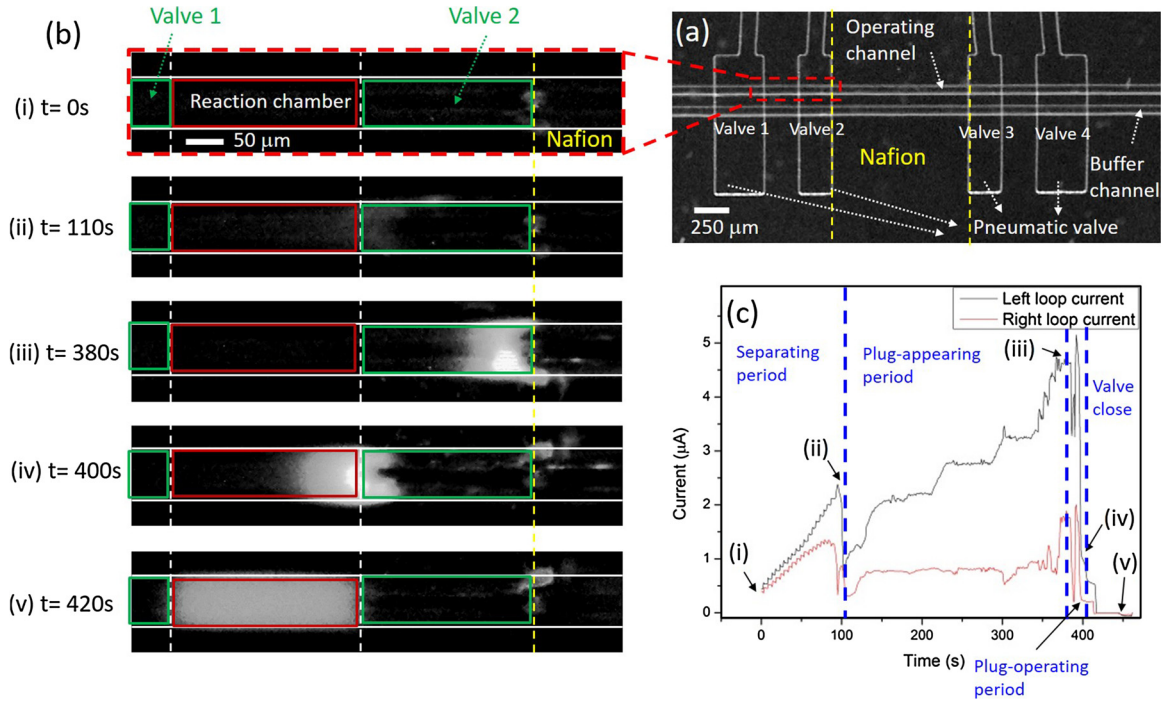

Fig. 3. Operational procedures of label-free nanofluidic preconcentration with pneumatic valves. (a) Overview of the device. A nanoporous thin film, composed of Nafion, is placed on the substrate and bridges the buffer channel and operating channel. The upper layer has four pneumatic valves, valves 1–4. If preconcentration is initiated on the left side of the depletion region, the protein plug is trapped between valves 1 and 2. Otherwise, the protein plug is trapped between valves 3 and 4. (b) Step-by-step visualization of protein collection, manipulation, and trapping. The entire process is also indicated in (c) the real-time current curve of the dual-loop preconcentrator. (i) Initially, the low-abundance fluorescent proteins in the microfluidic channel were barely observable. When the applied voltages reached 21 V, the currents of the left- and the right-loop circuits began to deviate, and the left-loop current was larger than the right-loop current; this phase is called the separation period. Simultaneously, the depletion region began to grow. (ii) As the depletion region became fully developed, the loop currents of both circuits drastically decreased. We continued to increase the voltages of both circuits: V_{left} was supplied a 10-V step voltage until a voltage of 70 V was achieved, and V_{right} was supplied a 1-V step voltage until a voltage of 45 V was achieved in 5 min. The results revealed that the left-loop current continuously increased with the increase in voltage; however, the right-loop current did not increase. In this period, the proteins continuously accumulated, and this phase is called the plug-appearance period. (iii) The proteins continuously accumulated to form a plug in approximately 5 min. (iv) The plug was moved to the interface between valve 2 and the reaction chamber by controlling voltages during the plug-operation period. (v) Finally, we pressurized the pneumatic valves to push the protein plug into the reaction chamber between valves 1 and 2.

captions of Fig. 3.

3.2. Brownian diffusivity measurements of nanobeads for PSA detection in microfluidic channel

To validate the preconcentrator-integrated immunobead biosensor, PSAs (P3338, Sigma-Aldrich) were used as test samples in this study. First, some preliminary experiments were performed to measure the interactions between PSA and anti-PSA by using 300-nm immunobeads at various PSA concentrations, including 0, 0.4, 0.8, 1.6, and 3.2 μg/ml. The anti-PSA-modified nanobeads, mixed with PSA solutions, were injected into the valve-integrated nanofluidic preconcentration device and isolated in the reaction chamber. The Brownian velocities of the nanobeads were measured through micro-PTV and the values were recorded every 10 s. The Brownian velocities of the nanobeads suspended in solution with no PSA showed a standard deviation of 0.1 μm/s, which is the systematic error of the micro-PTV measurements. When the nanobeads were suspended in various PSA solutions, the nanobeads' Brownian velocities showed a drastic reduction during a reaction period, and then reached an equilibrium state, which is named equilibrium Brownian velocity. During the reaction period, the standard deviation of Brownian velocities was larger than 0.1 μm/s, while when in the equilibrium state the standard deviation was obtained to be less than or equal to 0.1 μm/s. Fig. 4(a) exhibits the experimental results for the equilibrium Brownian velocities of the nanobeads, suspended in prepared PSA solutions. The standard deviation of the Brownian velocity for each condition was less than or equal to 0.1 μm/s. The averaged equilibrium Brownian velocity of nanobeads in a 0.4 μg/ml PSA solution was 5.4 μm/s, which was 0.3 μm/s less than the nanobeads' equilibrium Brownian velocity in solutions without PSA. We can conclude that 0.3 μm/s difference was three times larger than the systematic error of micro-PTV. The signal to noise ratio (SNR) was 3, and therefore we can also conclude that 0.4 μg/ml PSA solution was the detection limit of this nanobead measurement method. After the tests had been performed three times, a linearly fitted curve of the PSA concentration versus the Brownian velocity of the nanobeads at equilibrium was plotted as showed in Fig. 4(b). The coefficient of determination R^2 of the linear fitting line was approximately 96%, which indicates that the equilibrium Brownian velocity of the nanobeads was quite linearly related to the PSA concentration in the range of 0–3.2 μg/ml.

3.3. Protein preconcentration-enhanced PSA detection by nanobeads' Brownian diffusivity measurements

Bead-based immunoassays for sensing PSA samples at ultra-low concentrations were carried out by using protein preconcentration. Several PSA samples at various concentrations of 50, 100, 200, and 400 pg/ml were prepared. The mixtures containing anti-PSA-coated nanobeads and various PSA concentrations were injected into the preconcentration device. Initially, the Brownian velocities of the anti-PSA-modified nanobeads at different PSA concentrations without preconcentration were measured in the isolated reaction chamber in the region between valves 1 and 2 for 10 min because the valves were closed. In the second step, we opened the air valves. Simultaneously, we

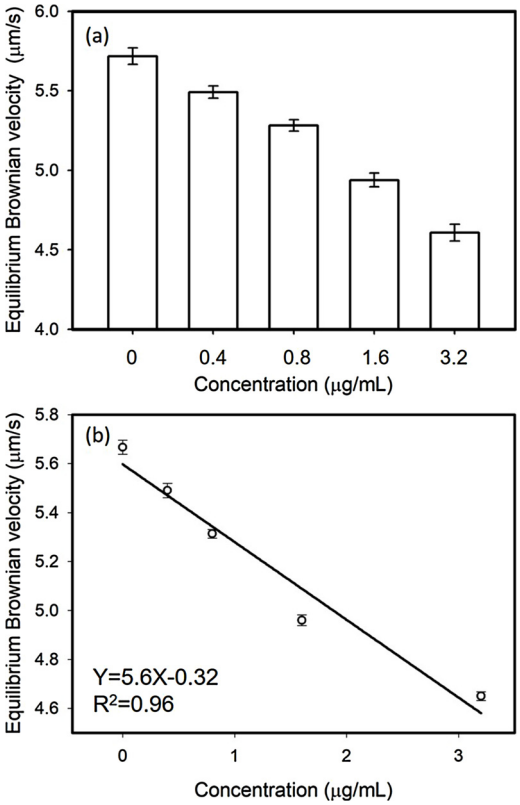

Fig. 4. (a) Equilibrium Brownian velocities of anti-PSA modified nanobeads suspended in different concentrations of PSA solutions. At a high PSA concentration in the range of 0–3.2 μg/ml, a drastic reduction in equilibrium Brownian velocities was observed. (b) Averaged results from three-time assays. The averaged equilibrium Brownian velocities of the nanobeads showed a linear decrease with the PSA concentration.

applied a voltage of 25 V to both dual-loop circuits to trigger the depletion region growth. As previously mentioned, the right- and the left-loop currents began to deviate, and the left-loop current was higher than the right-loop current in this experiment. Thus the concentration plug occurred on the left side of the Nafion membrane. Subsequently, both the loop currents drastically decreased. This indicated that the depletion region was fully developed. Thereafter, we directly applied voltages of 75 and 45 V to the left- and the right-loop circuits, respectively, for rapid protein accumulation. The entire processing time, including the depletion region growth and protein accumulation, was 90 s. By further applying a higher voltage difference between the two loop circuits and by pressurizing the pneumatic valves, the concentration plug and anti-PSA-modified nanobeads were moved into and trapped in the reaction chamber. At this stage, the concentrated PSA samples in the reaction chamber were detected by measuring the Brownian velocities of the nanobeads in real time.

Experimental results at four ultra-low PSA concentrations (50, 100, 200, and 400 pg/ml) with and without preconcentration are presented in Fig. 5. For the four samples without preconcentration, the equilibrium Brownian velocities of the nanobeads remained nearly the same value for 10 min. Similar results were obtained for nanobeads in solution without PSA as depicted in Fig. 4(a). A slight decrease (less than 0.1 μm/s) of equilibrium Brownian velocities was observed when PSA concentration was increased from 50 to 400 pg/ml. We speculated that the antibodies on the nanobeads interacted with PSA in the solutions, but the SNR was less than 1. With preconcentration, the Brownian velocities of the nanobeads in the four PSA samples decreased, furthermore, the equilibrium Brownian velocities were different. These results indicated that a higher PSA concentration leads to a lower Brownian velocity of nanobeads in the equilibrium state. Moreover, the

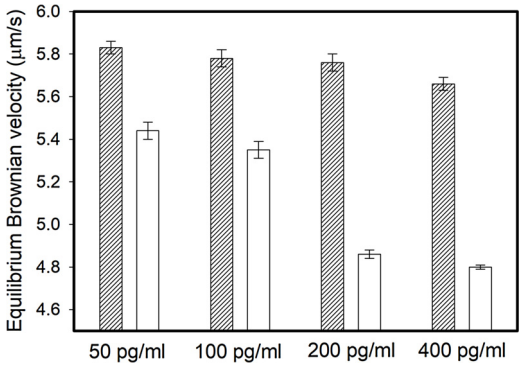

Fig. 5. Detection of low-abundance PSA samples at four concentrations of 50, 100, 200, and 400 pg/ml, with and without preconcentration. The dashed columns represent the sample detection without preconcentration, and the white columns are with preconcentration.

results revealed that the nanofluidic preconcentrator can be used to increase the detection limit of the bead-based immunoassay to the pg/ml level by measuring the Brownian diffusion of the nanobeads.

3.4. Preconcentration factor

After the Brownian velocities of nanobeads in preconcentrated PSA solutions had been measured three times, the averaged equilibrium Brownian velocities for the samples of various concentrations were obtained. These equilibrium Brownian velocities were plotted against the linear regression in Fig. 4(b), which is summarized in Fig. 6. Based on these results, the final concentrations of the ultra-low PSA samples after preconcentration can be estimated. We defined the final concentration over the original concentration of the sample as the preconcentration factor. In our experiments, the preconcentration factors of the prepared PSA samples at concentrations of 50, 100, 200, and 400 pg/ml were estimated as 7200 ± 800, 7800 ± 1000, 9500 ± 1000, and 7100 ± 800, respectively. Furthermore, according to these estimations, the average preconcentration factor of these four cases with this nanofluidic preconcentration device was determined as $7.90 \pm 0.9 \times 10^3$ in 90 s.

3.5. Sensing PSA in human serum

To validate the Brownian bead-immunosensing technique for detecting PSA in human serum, the PSA samples, diluted by human serum (H4522, Sigma-Aldrich), with seven various concentrations of 0, 0.75,

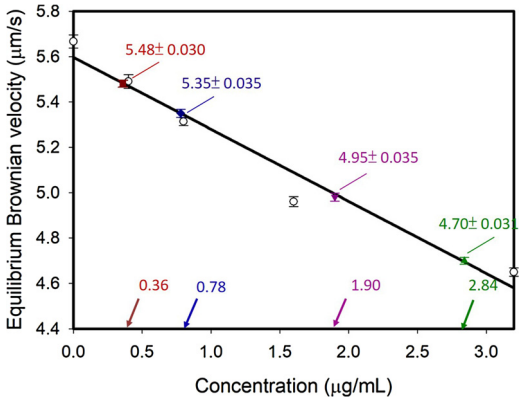

Fig. 6. Estimation of PSA concentration by comparing Brownian velocities measured at the equilibrium state and the linear regression of the bead-based immunoassay without preconcentration, as in Fig. 4(b). The PSA samples at concentrations of 50, 100, 200, and 400 pg/ml can be preconcentrated to 0.36, 0.78, 1.90, and 2.84 μg/ml, respectively.

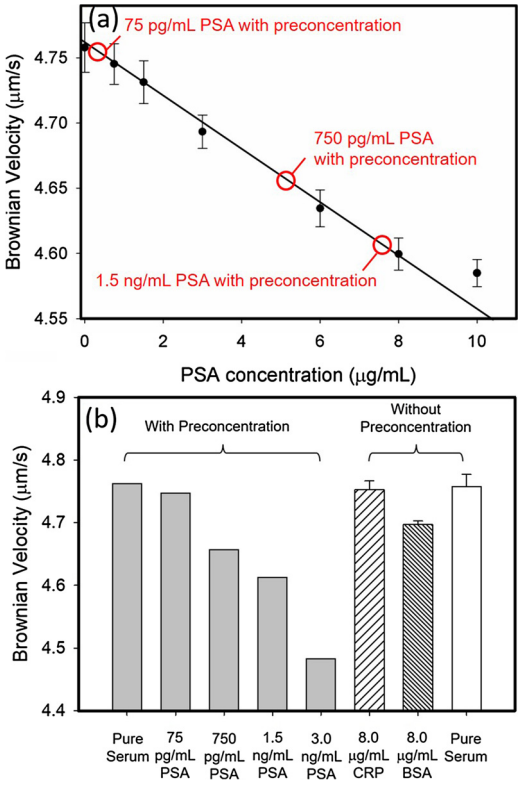

Fig. 7. Measurement results of PSA serum samples, (a) Equilibrium Brownian velocities of immunobeads suspended in different concentrations of PSA serum. A linear sensing range of 1–8 μg/ml was found. (b) The low-abundance PSA serum samples at concentration of 0, 0.075, 0.75, 1.5, 3 ng/ml were prepared to implement the preconcentrator integrated Brownian immunosesing technique. Further, the 8 μg/ml CRP and 8 μg/mL BSA serum samples were used for selectivity test.

1.5, 3.0, 6.0, 8.0, 10.0 μg/ml were prepared. The measurement results of Brownian velocities at equilibrium state of the anti-PSA-modified nanobeads in the PSA samples are shown in Fig. 7(a). The test for each concentration was conducted three times. When the PSA concentration in human serum is 0–10 μg/ml, the dynamic range of Brownian velocity at equilibrium state is in between 4.58–4.75 μm/s, which is about 1 μm/s less than that in PBS solution. The reason is that the viscosity of the human serum is around 1.5 cP, which is higher than that of the PBS solution. The higher viscosity of the surrounding medium is, the lower the Brownian diffusivity is, and the dynamic range becomes smaller as well. Further, when the PSA concentation is between 1 and 8 μg/ml, a linear dynamic range of the Brownian velocity can be approximately observed.

Concerning the preconcentration enhancement test, various PSA concentrations of 0.075, 0.75, 1.5, and 3 ng/ml were prepared for the experiments. The preconcentration processes were also followed the same procedures as in section 2.3. The mixtures containing anti-PSA-coated nanobeads and PSA serum solutions with various concentrations were injected into the preconcentration device. After preconcentration, valve-closing, and measurement, the immunobeads' Brownian velocities in various PSA solutions at equilibrium state are shown in Fig. 7(b). The results are also labeled in Fig. 7(a) to indicate the enhanced concentrations. The immunobeads' equilibrium Brownian velocity in preconcentrated 75 pg/ml PSA serum was similar to that in pure serum without preconcentration. The immunobeads' equilibrium Brownian velocity in preconcentrated 750 pg/ml and 1.5 ng/ml PSA serum showed similar to those in 5 μg/ml and 7.8 μg/ml without preconcentration, respectively. This result indicates that the preconcentration factors are 6600 and 5200, respectively. Furthermore, for preconcentrated 3.0 ng/ml PSA serum, the immunobeads' equilibrium Brownian velocity was out of the dynamic range. During the same processing time, the preconcentration factors in human serum are smaller than those in PBS solutions, because the electroosmotic force was weaker in higher viscosity liquid in a microfluidic channel.

A selectivity test was also implemented. We prepared two test samples which included 8 μg/ml C-reactive protein (CRP) in human serum, and 8 μg/ml bovine serum albumin (BSA) in human serum. The immunobeads were suspended in these two samples and the measurement results are also shown in Fig. 7(b) comparing with the results in the pure serum sample. From these results, we found that the Brownian velocity of the immunobeads in pure serum samples at equilibrium state didn't show much difference from those in CRP samples. Further, the Brownian velocity was found to be lower when in BSA samples. These results indicate that the anti-PSAs on the immunobeads partially interacted with BSA, and leads to that the immunobeads' Brownian velocity will decrease. However, the BSA will not be found in human serum in general.

4. Conclusions

A highly sensitive bead-based immunoassay integrated with a nanofluidic preconcentration device was successfully developed in this study. By using pneumatic valves, the antibody-modified immunobeads and concentrated antigens can be trapped in a small reaction chamber for further detection. The antibody–antigen interactions can be determined by directly measuring the diffusivity of the immunobeads in a 10-min period. At a higher concentration of antigens, the antibody-modified immunobeads yielded lower equilibrium Brownian velocities in the sensing range. By using the nanofluidic preconcentration device, the preconcentration process can be completed in 90 s, and a PSA detection limit as low as 50 pg/ml can be achieved. An average preconcentration factor of $7.9 \pm 0.9 \times 10^3$ was estimated in our experiment. Furthermore, the PSA samples in the range of 50–400 pg/ml can be preconcentrated to 0–3.2 μg/ml, which is within the detection range of a conventional 3D bead-based immunoassay using micro-PTV for measuring the Brownian velocities of nanobeads. The entire process, including preconcentration and measurement, can be completed in 20 min.

The measurement technique was also implemented in various PSA concentration in human serum. Without preconcentration, a linear sensing range of 1–8 μg/ml was found. After precocnentration, 0.1–2 ng/ml PSA samples can be detected. When PSA concentration is over 2 ng/ml, the immunobeads' Brownian velocity will reach saturation state. Approximately 75% of the cancers were detected when PSA concentration in serum is higher than 2 ng/ml; furthermore, approximately 13–22% of men have a prostate cancer detectable by biopsy and 80–85% of these are organ confined [35–37]. This method can rapidly screen the PSA in a healthy range, and show overloaded when the PSA concentration is in a dangerous region.

Acknowledgements

This work was supported by the Ministry of Science and Technology of Taiwan under grant numbers MOST 105-2221-E-002-102 and 104-2221-E-002-111 and by Taipei Medical University under grant number TMU105-AE1-B51. We would also like to thank the NEMS Research Center, National Taiwan University for facility support.

Appendix A. Supplementary data

Supplementary data associated with this article can be found, in the online version, at https://doi.org/10.1016/j.snb.2018.05.141.

References

[1] D.A. Healy, C.J. Hayes, P. Leonard, L. McKenna, R. O'Kennedy, Biosensor developments: application to prostate-specific antigen detection, Trends Biotechnol. 25 (2007) 125–131.

[2] H.A. Ahmed, H.M. Azzazy, Power-free chip enzyme immunoassay for detection of prostate specific antigen (PSA) in serum, Biosens. Bioelectrons 49 (2013) 478–484.

[3] Z. Ye, M. Tan, G. Wang, J. Yuan, Preparation, characterization, and time-resolved fluorometric application of silica-coated terbium (III) fluorescent nanoparticles, Anal. Chem. 76 (2004) 513–518.

[4] P. Huhtinen, T. Soukka, T. Lövgren, H. Härmä, Immunoassay of total prostate-specific antigen using europium (III) nanoparticle labels and streptavidin-biotin technology, J. Immunol. Methods 294 (2004) 111–122.

[5] D.S. Grubisha, R.J. Lipert, H.-Y. Park, J. Driskell, M.D. Porter, Femtomolar detection of prostate-specific antigen: an immunoassay based on surface-enhanced Raman scattering and immunogold labels, Anal. Chem. 75 (2003) 5936–5943.

[6] C. Cao, J.P. Kim, B.W. Kim, H. Chae, H.C. Yoon, S.S. Yang, et al., A strategy for sensitivity and specificity enhancements in prostate specific antigen-α 1-antichymotrypsin detection based on surface plasmon resonance, Biosens. Bioelectrons 21 (2006) 2106–2113.

[7] G. Wu, R.H. Datar, K.M. Hansen, T. Thundat, R.J. Cote, A. Majumdar, Bioassay of prostate-specific antigen (PSA) using microcantilevers, Nat. Biotechnol. 19 (2001) 856–860.

[8] D.-J. Kim, N.-E. Lee, J.-S. Park, I.-J. Park, J.-G. Kim, H.J. Cho, Organic electrochemical transistor based immunosensor for prostate specific antigen (PSA) detection using gold nanoparticles for signal amplification, Biosens. Bioelectrons 25 (2010) 2477–2482.

[9] G. Zheng, F. Patolsky, Y. Cui, W.U. Wang, C.M. Lieber, Multiplexed electrical detection of cancer markers with nanowire sensor arrays, Nat. Biotechnol. 23 (2005) 1294–1301.

[10] G. Pampalakis, S.O. Kelley, An electrochemical immunosensor based on antibody-nanowire conjugates, Analyst 134 (2009) 447–449.

[11] C. Li, M. Curreli, H. Lin, B. Lei, F. Ishikawa, R. Datar, et al., Complementary detection of prostate-specific antigen using In2O3 nanowires and carbon nanotubes, J. Am. Chem. Soc. 127 (2005) 12484–12485.

[12] J. Okuno, K. Maehashi, K. Kerman, Y. Takamura, K. Matsumoto, E. Tamiya, Label-free immunosensor for prostate-specific antigen based on single-walled carbon nanotube array-modified microelectrodes, Biosens. Bioelectrons 22 (2007) 2377–2381.

[13] L.F. Cheow, S.H. Ko, S.J. Kim, K.H. Kang, J. Han, Increasing the sensitivity of enzyme-linked immunosorbent assay using multiplexed electrokinetic concentrator, Anal. Chem. 82 (2010) 3383–3388.

[14] J.H. Lee, Y.-A. Song, J. Han, Multiplexed proteomic sample preconcentration device using surface-patterned ion-selective membrane, Lab Chip 8 (2008) 596–601.

[15] K.-B. Sung, K.-P. Liao, Y.-L. Liu, W.-C. Tian, Development of a nanofluidic preconcentrator with precise sample positioning and multi-channel preconcentration, Microfluid. Nanofluid. 14 (2013) 645–655.

[16] Y.-C. Wang, A.L. Stevens, J. Han, Million-fold preconcentration of proteins and peptides by nanofluidic filter, Anal. Chem. 77 (2005) 4293–4299.

[17] P.-S. Chung, Y.-J. Fan, H.-J. Sheen, W.-C. Tian, Real-time dual-loop electric current measurement for label-free nanofluidic preconcentration chip, Lab Chip 15 (2015) 319–330.

[18] Y.-C. Wang, J. Han, Pre-binding dynamic range and sensitivity enhancement for immuno-sensors using nanofluidic preconcentrator, Lab Chip 8 (2008) 392–394.

[19] J.H. Lee, Y.-A. Song, S.R. Tannenbaum, J. Han, Increase of reaction rate and sensitivity of low-abundance enzyme assay using micro/nanofluidic preconcentration chip, Anal. Chem. 80 (2008) 3198–3204.

[20] J.H. Lee, B.D. Cosgrove, D.A. Lauffenburger, J. Han, Microfluidic concentration-enhanced cellular kinase activity assay, J. Am. Chem. Soc. 131 (2009) 10340–10341.

[21] S.H. Ko, Y.-A. Song, S.J. Kim, M. Kim, J. Han, K.H. Kang, Nanofluidic preconcentration device in a straight microchannel using ion concentration polarization, Lab Chip 12 (2012) 4472–4482.

[22] Y.-J. Fan, H.-J. Sheen, C.-J. Hsu, C.-P. Liu, S. Lin, K.-C. Wu, A quantitative immunosensing technique based on the measurement of nanobeads' Brownian motion, Biosens. Bioelectrons 25 (2009) 688–694.

[23] Y.-J. Fan, H.-J. Sheen, Y.-H. Liu, J.-F. Tsai, T.-H. Wu, K.-C. Wu, et al., Detection of C-reactive protein in evanescent wave field using microparticle-tracking velocimetry, Langmuir 26 (2010) 13751–13754.

[24] Y.-J. Fan, Y.-C. Chang, C.-T. Teng, T.-Y. Liao, W.-C. Hu, H.-J. Sheen, Detection of orchid viruses by analyzing Brownian diffusion of nanobeads and virus-immunobead association, Anal. Methods 7 (2015) 5476–5482.

[25] V.M. Gorti, H. Shang, S.T. Wereley, G.U. Lee, Immunoassays in nanoliter volume reactors using fluorescent particle diffusometry, Langmuir 24 (2008) 2947–2952.

[26] C.-Y. Chung, J.-C. Wang, H.-S. Chuang, Rapid bead-based antimicrobial susceptibility testing by optical diffusometry, PLoS One 11 (2016) e0148864.

[27] Y.-J. Fan, H.-J. Sheen, Z.-Y. Chen, Y.-H. Liu, J.-F. Tsai, K.-C. Wu, TIRF-enhanced nanobeads' Brownian diffusion measurements for detecting CRP in human serum, Microfluid. Nanofluid. 19 (2015) 85–94.

[28] K.N. Clayton, J.W. Salameh, S.T. Wereley, T.L. Kinzer-Ursem, Physical characterization of nanoparticle size and surface modification using particle scattering diffusometry, Biomicrofluidics 10 (2016) 054107.

[29] Q. Pu, J. Yun, H. Temkin, S. Liu, Ion-enrichment and ion-depletion effect of nanochannel structures, Nano Lett. 4 (2004) 1099–1103.

[30] F.C. Leinweber, U. Tallarek, Nonequilibrium electrokinetic effects in beds of ion-permselective particles, Langmuir 20 (2004) 11637–11648.

[31] R.B. Schoch, J. Han, P. Renaud, Transport phenomena in nanofluidics, Rev. Mod. Phys. 80 (2008) 839.

[32] I. Rubinstein, B. Zaltzman, Electro-osmotically induced convection at a permselective membrane, Phys. Rev. E 62 (2000) 2238.

[33] J.H. Lee, S. Chung, S.J. Kim, J. Han, Poly (dimethylsiloxane)-based protein preconcentration using a nanogap generated by junction gap breakdown, Anal. Chem. 79 (2007) 6868–6873.

[34] D. Mark, S. Haeberle, G. Roth, F. von Stetten, R. Zengerle, Microfluidic lab-on-a-chip platforms: requirements, characteristics and applications, Chem. Soc. Rev. 39 (2010) 1153–1182.

[35] H.J. Linton, L.S. Marks, L.S. Millar, C.L. Knott, H.G. Rittenhouse, S.D. Mikolajczyk, Benign prostate-specific antigen (BPSA) in serum is increased in benign prostate disease, Clin. Chem. 49 (2003) 253–259.

[36] A.W. Roddam, M.J. Duffy, F.C. Hamdy, A.M. Ward, J. Patnick, C.P. Price, et al., Use of prostate-specific antigen (PSA) isoforms for the detection of prostate cancer in men with a PSA level of 2–10 ng/ml: systematic review and meta-analysis, Eur. Urol. 48 (2005) 386–399.

[37] I. Thompson, D. Ankerst, C. Chi, M. Lucia, P. Goodman, J. Crowley, et al., Operating characteristics of prostate-specific antigen in men with an initial PSA level of 3.0 Ng/Ml or lower, J. Urol. 175 (2006) 562–563.

Dr. Yu-Jui Fan is currently an assistant professor in College of Biomedical Engineering, Taipei Meidical University. His research interest is focusing on electrical and optical based in vitro diagnostic devices.

Chih-Zong Deng received his BS degree from Department of Aeronautics and Astronautics, National Cheng Kung University in 2014, and MS degree from Institute of Applied Mechanics, National Taiwan University in 2016. He is currently a research assistant in National Taiwan University.

Pei-Shang Chung received his BS degree from Department of Electrical Engineering, National Taiwan University in 2011, and MS degree from Graduate Institute of Biomedical Electronics and Bioinformates, National Taiwan University in 2013. She is currently a PhD student in Department of Bioengineering, University of California, Los Angeles (UCLA).

Dr. Wei-Cheng Tian is currently an associate professor in Department of Electrical Engineering, Graduate Institute of Electronics Engineering, and Graduate Institute of Biomedical Electronics and Bioinformates, National Taiwan University. His research interests are on biological, chemical, and medical applications of micro & nano technologies with the focus on the CMOS compatible integration, packaging, and reliability of the micro/nano devices and systems.

Dr. Horn-Jiunn Sheen is currently a professor in the Institute of Applied Mechanics, National Taiwan University. His research interests include micro-fluidics, bio-sensors, and flow measurements. The main research equipment and facilities in his laboratory are flow visualization systems, laser-Doppler velocimetry, and micro-Particle Tacking/Image Velocimetry.